Dual-band spectral-domain optical coherence tomography for *in vivo* imaging the spectral contrasts of the retinal nerve fiber layer

Xiangyang Zhang,[1] Jianming Hu,[1,3] Robert W. Knighton,[2] Xiang-Run Huang,[2] Carmen A. Puliafito,[1] and Shuliang Jiao[1,*]

[1]*Department of Ophthalmology, Keck School of Medicine, University of Southern California, Los Angeles, CA 90033, USA*
[2]*Bascom Palmer Eye Institute, University of Miami Miller School of Medicine, Miami, FL 33136, USA*
[3]*Chongqing Key Laboratory of Optics and Engineering, Chongqing Normal University, Chongqing 40047, China*
[*]*sjiao@usc.edu*

Abstract: The ultimate goal of the study is to provide an imaging tool to detect the earliest signs of glaucoma before clinically visible damage occurs to the retinal nerve fiber layer (RNFL). Studies have shown that the optical reflectance of the damaged RNFL at short wavelength (<560nm) is reduced much more than that at long wavelength, which provides spectral contrast for imaging the earliest damage to the RNFL. To image the spectral contrast we built a dual-band spectral-domain optical coherence tomography (SD-OCT) centered at 808nm (NIR) and 415nm (VIS). The light at the two bands was provided by the fundamental and frequency-doubled outputs of a broadband Ti:Sapphire laser. The depth resolution of the NIR and VIS OCT systems are 4.7μm and 12.2μm in the air, respectively. The system was applied to imaging the rat retina *in vivo*. Significantly different appearances between the OCT cross sectional images at the two bands were observed. The ratio of the light reflected from the RNFL over that reflected from the entire retina at the two bands were quantitatively compared. The experimental results showed that the dual-band OCT system is feasible for imaging the spectral contrasts of the RNFL.

OCIS codes: (170.0170) Medical optics and biotechnology; (170.1610) Clinical applications; (170.4460) Ophthalmic optics and devices; (170.4500) Optical coherence tomography; (170.4580) Optical diagnostics for medicine.

References and links

1. H. A. Quigley, "Glaucoma," Lancet **377**(9774), 1367–1377 (2011).
2. L. A. Kerrigan-Baumrind, H. A. Quigley, M. E. Pease, D. F. Kerrigan, and R. S. Mitchell, "Number of ganglion cells in glaucoma eyes compared with threshold visual field tests in the same persons," Invest. Ophthalmol. Vis. Sci. **41**(3), 741–748 (2000).
3. M. L. Gabriele, G. Wollstein, H. Ishikawa, L. Kagemann, J. Xu, L. S. Folio, and J. S. Schuman, "Optical coherence tomography: history, current status, and laboratory work," Invest. Ophthalmol. Vis. Sci. **52**(5), 2425–2436 (2011).
4. H. G. Lemij and N. J. Reus, "New developments in scanning laser polarimetry for glaucoma," Curr. Opin. Ophthalmol. **19**(2), 136–140 (2008).
5. R. W. Knighton, X. Huang, and Q. Zhou, "Microtubule contribution to the reflectance of the retinal nerve fiber layer," Invest. Ophthalmol. Vis. Sci. **39**(1), 189–193 (1998).
6. X.-R. Huang and R. W. Knighton, "Microtubules contribute to the birefringence of the retinal nerve fiber layer," Invest. Ophthalmol. Vis. Sci. **46**(12), 4588–4593 (2005).
7. B. Fortune, L. Wang, G. Cull, and G. A. Cioffi, "Intravitreal colchicine causes decreased RNFL birefringence without altering RNFL thickness," Invest. Ophthalmol. Vis. Sci. **49**(1), 255–261 (2008).
8. G. M. Pocock, R. G. Aranibar, N. J. Kemp, C. S. Specht, M. K. Markey, and H. G. Rylander 3rd, "The relationship between retinal ganglion cell axon constituents and retinal nerve fiber layer birefringence in the primate," Invest. Ophthalmol. Vis. Sci. **50**(11), 5238–5246 (2009).
9. X.-R. Huang and R. W. Knighton, "Altered F-actin distribution in retinal nerve fiber layer of a rat model of glaucoma," Exp. Eye Res. **88**(6), 1107–1114 (2009).

#152410 - $15.00 USD Received 4 Aug 2011; revised 12 Sep 2011; accepted 15 Sep 2011; published 22 Sep 2011

10. X.-R. Huang, W. Kong, Y. Zhou, and G. Gregori, "Distortion of axonal cytoskeleton: an early sign of glaucomatous damage," Invest. Ophthalmol. Vis. Sci. **52**(6), 2879–2888 (2011).
11. X.-R. Huang, Y. Zhou, W. Kong, and R. W. Knighton, "Reflectance decrease prior to thickness change of the retinal nerve fiber layer in glaucomatous retinas", Invest. Ophthalmol. Vis. Sci., published ahead of print July 5, 2011.
12. R. W. Knighton and X.-R. Huang, "Directional and spectral reflectance of the rat retinal nerve fiber layer," Invest. Ophthalmol. Vis. Sci. **40**(3), 639–647 (1999).
13. X.-R. Huang, Y. Zhou, W. Kong, and R. W. Knighton, "Change of retinal nerve fiber layer reflectance correlated with cytostructural change in glaucoma," ARVO Meeting Abstracts (Fort Lauderdale, Florida 2011), 52:2442.
14. M. Ruggeri, G. Tsechpenakis, S. Jiao, M. E. Jockovich, C. Cebulla, E. Hernandez, T. G. Murray, and C. A. Puliafito, "Retinal tumor imaging and volume quantification in mouse model using spectral-domain optical coherence tomography," Opt. Express **17**(5), 4074–4083 (2009).
15. X. Zhang, H. F. Zhang, C. A. Puliafito, and S. Jiao, "Simultaneous in vivo imaging of melanin and lipofuscin in the retina with photoacoustic ophthalmoscopy and autofluorescence imaging," J. Biomed. Opt. **16**(8), 080504 (2011).
16. R. W. Knighton and X.-R. Huang, "Visible and near-infrared imaging of the nerve fiber layer of the isolated rat retina," J. Glaucoma **8**(1), 31–37 (1999).
17. Scott Prahl, "Optical Absorption of Hemoglobin," *http://omlc.ogi.edu/spectra/hemoglobin/summary.html*.

1. Introduction

Glaucoma, one of the leading causes of irreversible blindness worldwide, occurs when the retinal ganglion cells and their axons in the retinal nerve fiber layer (RNFL) and optic nerve degenerate in a characteristic and identifiable pattern called glaucomatous optic neuropathy (recently reviewed in Ref. 1). Untreated glaucoma may lead to permanent loss of vision, which motivates attempts to detect the earliest signs of the disease. Early diagnosis will permit early medical intervention to prevent vision loss. Current clinical methods for glaucoma diagnosis detect degenerative damage after it has already occurred, either structural damage (tissue loss in the optic disc, RNFL or macula) or functional damage (loss of visual sensitivity). Some data suggest that structural damage can occur many years before detectable loss of visual sensitivity [2] and a variety of optical approaches to structural assessment have been pursued. In particular, recent advances in optical coherence tomography (OCT) for glaucoma diagnosis have mostly focused on structural measurements [3].

In the case of the RNFL, some clinical and laboratory methods have progressed beyond the measurement of structure to the assessment of the optical properties of the tissue. For example, the commercially available technology of scanning laser polarimetry uses retardation by RNFL birefringence as a measure of RNFL integrity [4]. The optical properties of the RNFL depend on axonal structure at the submicroscopic level; its birefringence, for example, arises from parallel intracellular fibrils called microtubules [5–8]. Importantly, studies of the RNFL in a rat model of glaucoma show that the axonal cytoskeleton can change before the decrease in RNFL thickness [9,10] and in pilot studies we used high resolution small animal OCT operating at a center wavelength of 830 nm to confirm that there was no decrease in the RNFL thickness measured *in vivo* for the same rats (data unpublished). Even more promising, RNFL reflectance can decline before histologically detectable change in the axonal cytoskeleton [11]. Thus, the measurement of RNFL optical properties may allow a means to detect changes in cellular substructure that occur before axonal degeneration. This in turn could lead to diagnostic methods that reveal a therapeutic window during which permanent damage might be prevented.

The RNFL reflectance at all wavelengths arises from light scattering by cylindrical structures, with RNFL reflectance spectra suggesting the presence of at least two scattering mechanisms [12]. The spectra can be fit by a model where the reflectance at wavelengths shorter than 570 nm comes from cylinders with diameters much smaller than the wavelength, but the reflectance at wavelengths longer than ~680 nm comes from cylinders with effective diameters of 350 nm to 900 nm. A recent report showed that the RNFL reflectance in the rat glaucoma model also demonstrated spectral changes; at short wavelengths (< 560nm) the reflectance of the affected RNFL decreased much more than at long wavelengths [13]. This result suggests that the subtle structural alteration of axons in early glaucoma produces a wavelength dependent change in the RNFL reflectance.

#152410 - $15.00 USD Received 4 Aug 2011; revised 12 Sep 2011; accepted 15 Sep 2011; published 22 Sep 2011

In conventional ophthalmic OCT, the RNFL appears as a brightly reflecting layer. Because the light sources used in ophthalmic OCT systems are in the near infrared (NIR), the detected light from the RNFL should come mainly from scattering by thick cylindrical structures, making NIR OCT intrinsically insensitive to the very early changes seen in the rat model of glaucoma. If we shift the wavelength of the OCT to the visible (shorter than 570 nm), however, the changes to the thin cylindrical structures may be detectable. Ideally, an OCT system that covers both long and short wavelengths should be able to image contributions from both the thin and thick cylindrical structures in the nerve fibers. To test this hypothesis, an OCT system working in the visible spectrum (preferably at a center wavelength < 500 nm) is needed.

In this paper we report on our first effort in building and testing an OCT system working at a center wavelength of ~415 nm specifically for imaging the spectral contrast of the RNFL. The current study is a technical preparation for investigations on early diagnosis and progressive assessment of glaucoma using imaging technologies.

2. Experimental system

Figure 1 shows a schematic of the experimental system. The system consists of two spectral-domain OCT systems: one working in the NIR band and the other one working in the visible (VIS) band. A broadband Ti: Sapphire laser (MICRA, center wavelength: 800 nm, bandwidth: 120 nm, Coherent Inc, USA) was used as the fundamental light source. A frequency doubling crystal (BBO, Castech, Fujian, China) was used to convert the laser light to the visible. To ensure a broadband output from the crystal the fundamental laser light was focused into the crystal by a lens of f=14 mm (L1). The light exiting the BBO crystal was first collimated with an achromatic lens of f=40 mm (L2) and then reflected by a long-pass filter (FEL0700, Thorlabs, USA) to separate the visible light from the residual fundamental light.

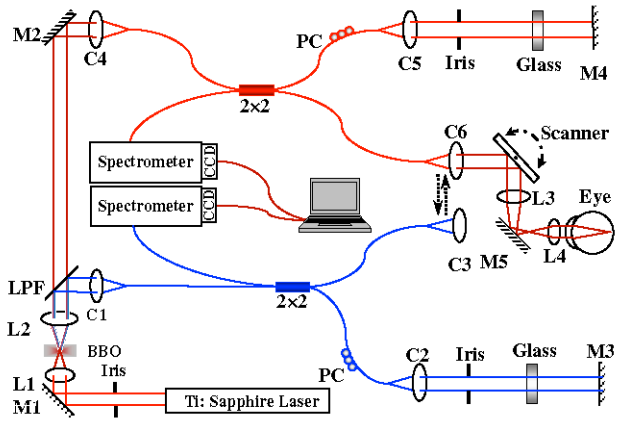

Fig. 1. Schematic of the dual-band OCT system. M1~M5: mirror; L1~L4: lens; BBO: BBO crystal; LPF: long-pass filter. C1~C6: Collimator; PC: Polarization Controller.

The visible light was then coupled into the source arm of a single mode optical fiber-based Michelson interferometer. In the detection arm the reflected light from the sample and reference arms was collimated and detected by a spectrometer, which consisted of an 1800 line/mm transmission grating, a multi-element imaging lens (f=150 mm), and a line scan CCD camera (Aviiva-SM2-CL-2010, 2048 pixels with 10 micron pixel size operating in 12-bit mode, e2V). An image acquisition board (NI IMAQ PCI 1428) acquired the image captured by the camera and transferred it to a workstation (HP xw4600, 4 GB memory) for signal processing and image display. The design of the NIR-OCT is similar to that in our previous publications [14,15] except that the residual fundamental light after the long-pass filter was used as the light source.

#152410 - $15.00 USD Received 4 Aug 2011; revised 12 Sep 2011; accepted 15 Sep 2011; published 22 Sep 2011

After exiting their corresponding optical fibers in the sample arms the visible and NIR probing light beams were collimated with collimators that can be interchangeably connected with the scanning and optical delivery system. The scanning and optical delivery system was built on a modified slit lamp. The probing light beams were scanned by an X-Y galvanometer scanner and delivered to the eye through an achromatic relay lens (f = 75 mm) and an objective lens (f = 19 mm).

3. Results and discussion

3.1 Spectral reflectance of the RNFL

We measured the spectral reflectance of the RNFL of living *ex vivo* rat retinas by using imaging micro-reflectometry (IMR) [13,16]. The result of measurement is shown in Fig. 2. Rectangular areas are defined both on a nerve fiber bundle (black boxes) and nearby gaps (white boxes), where no nerve fiber bundles exist. The average reflected light intensity of both bundle (I_b) and gap (I_g) areas are calculated. Reflectance from RNFL only is then derived as $I = I_b - I_g$. Figure 2B shows the RNFL spectral reflectance of a glaucomatous eye and its control eye in a rat glaucoma model produced by laser treatment of the trabecular meshwork [9–11]. Intra-ocular pressure (IOP) before treatment for both eyes was 24 mmHg. The treated eye was exposed to high IOP for 18 days with peak IOP of 48 mmHg. The spectra were measured 4 weeks after the start of treatment. The experiments showed that glaucoma causes decreased RNFL reflectance at short wavelengths while it remained approximately the same at longer wavelengths.

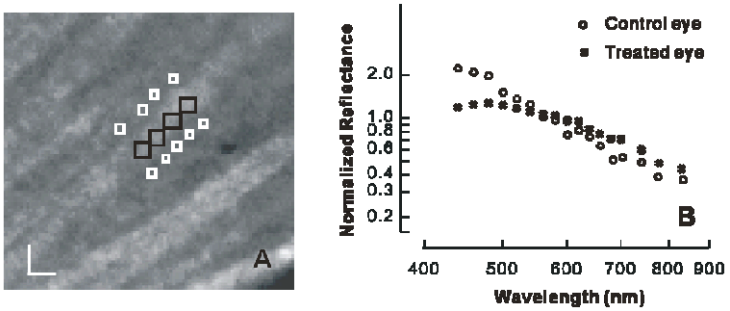

Fig. 2. Measurement of RNFL reflectance. A: typical reflection image of the RNFL; nerve fiber bundles appear as bright stripes; B: calculated spectral reflectance of the RNFL; Bar: 20 μm.

3.2 VIS-OCT experiments

Figure 3 shows the measured spectra and the point-spread functions of the two OCT systems. The center wavelength and full width at half maximum (FWHM) of the NIR light are 808 nm and about 105 nm, respectively. The NIR-OCT achieved a depth resolution of about 4.7 μm and an imaging depth of 2.5 mm in the air. The center wavelength and FWHM of the visible light are 415 nm and 7 nm, respectively. The VIS-OCT achieved a depth resolution of about 12.2 μm and an imaging depth of 1.3 mm in the air.

The system was applied to imaging the normal rat retina *in vivo*. The animals (Sprague Dawley rats, body weight: 600~750 g, Charles Rivers) were anesthetized by intraperitoneal injection of a cocktail containing ketamine (54 mg/kg body weight) and xylazine (6 mg/kg body weight). In the meantime, the pupils were dilated with 10% phenylephrine solution. Drops of artificial tears were applied to the eyes every two minutes to prevent dehydration of the cornea and cataract formation. After anesthetization, the animals were restrained in a mounting tube, which was fixed on a five-axis platform. Raster scans with the fast axis along the horizontal direction were performed. All experiments were performed in compliance with the guidelines of the University of Southern California's Institutional Animal Care and Use Committee.

#152410 - $15.00 USD Received 4 Aug 2011; revised 12 Sep 2011; accepted 15 Sep 2011; published 22 Sep 2011

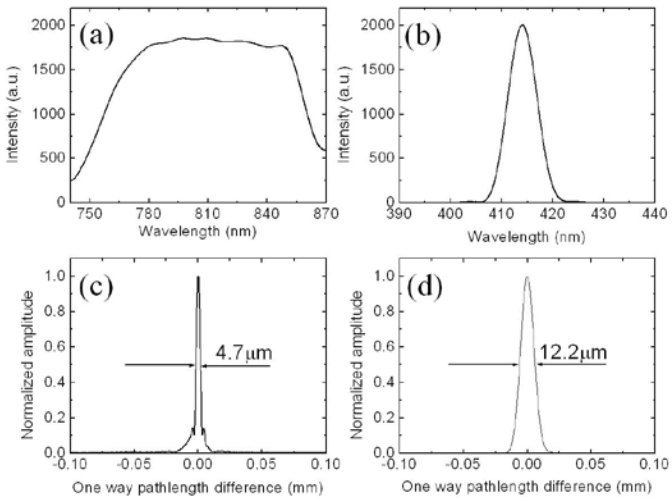

Fig. 3. Measured parameters of the NIR and VIS OCT systems. (a) and (b): spectra of the NIR and VIS OCT systems; (c) and (d): PSF of the NIR and VIS OCT systems.

In the experiment, we collected the NIR and VIS-OCT images sequentially. The initial alignment including finding the area of interest was done with the NIR OCT. After the acquisition of the NIR OCT image we mechanically switched the VIS OCT into position and acquired the VIS OCT images. In our current study the laser energy after the objective lens was measured to be 450 μw for the visible and 750 μw for the NIR light, which are both below the ANSI safety limits for eye imaging. Since the OCT images of the two different bands were not acquired simultaneously they are not completely registered due to movement of the animal during the switching process. The advantage of using the NIR-OCT for alignment is to reduce the retinal exposure to the visible light. The higher axial resolution and greater imaging depth of the NIR-OCT also aided the alignment.

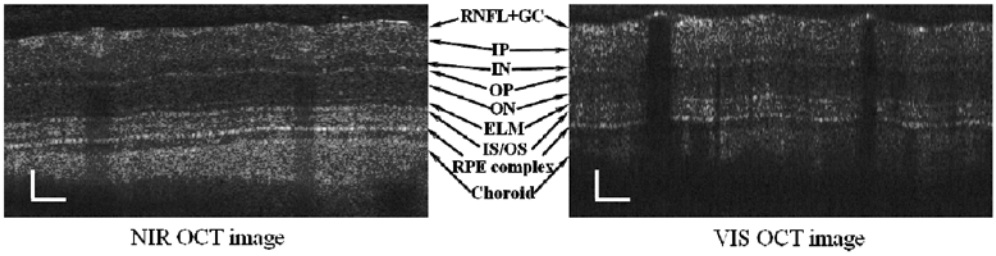

Fig. 4. Sample images of a rat retina acquired with the NIR OCT and VIS OCT. Images consist of 2048 A-lines. Bar: 100 μm.

Figure 4 shows one pair of the acquired NIR and VIS OCT images. The images consist of 2048 A-scans and cover a length of about 1.3 mm across the retina. The differences between the NIR and VIS OCT images are significant. As expected the blood vessels blocked the VIS probing light completely with only reflections from their front boundaries, while the NIR-OCT still revealed some features beneath the vessels. This difference comes from the significant difference of the absorption coefficients of hemoglobin at the two bands: at 415 nm μ_a = 2801.52 (cm^{-1}) for oxy-hemoglobin (HbO_2) and μ_a = 1891.79 (cm^{-1}) for deoxy-hemoglobin (Hb); at 808 nm μ_a = 4.58 (cm^{-1}) for HbO2 and μ_a = 3.88 (cm^{-1}) for Hb [17].

#152410 - $15.00 USD Received 4 Aug 2011; revised 12 Sep 2011; accepted 15 Sep 2011; published 22 Sep 2011

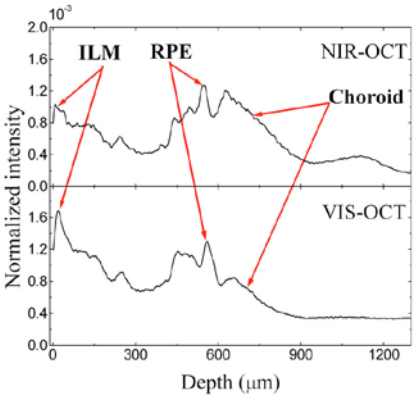

Fig. 5. Normalized average of the A-lines of the OCT images in Fig. 4.

In the NIR OCT image there are strong signals from deep into the choroid. In the VIS OCT image, although we can still recognize all the retinal layers there are much weaker signals from behind the RPE layer due to the higher attenuation coefficient of the RPE in the VIS band. To further demonstrate the different characteristics of the OCT signal in the two bands we averaged all the A-lines of the images in Fig. 4. Before averaging we flattened each image by first drawing their ILMs and then shifting each A-line in the depth direction accordingly. The averaged A-lines are shown in Fig. 5. From Fig. 4 and Fig. 5 we can see that the RPE signal is the strongest in the NIR OCT image. In contrast, the RNFL signal is the strongest in the VIS OCT image. Another noticeable feature is that the boundaries among the different retinal layers in the VIS OCT image are not as clear as those in the NIR OCT image. This feature may be caused by the different depth resolutions of the two OCT systems. Other factors like the differences of the optical properties, e.g. index of refraction of the different layers in the VIS and NIR bands may also play a role.

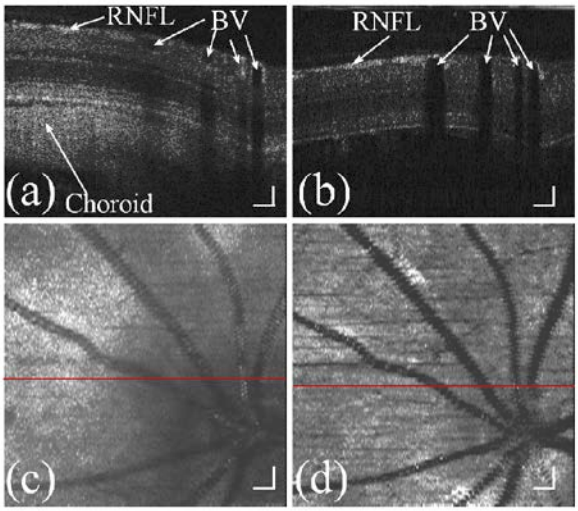

Fig. 6. Retinal images acquired with the NIR and VIS OCT systems. (a): B-scan image of the NIR OCT; (b): B-scan image of the VIS OCT; (c): NIR-OCT fundus image; (d): VIS-OCT fundus image. BV: blood vessel. Bar: 100 μm.

Figure 6 shows another typical pair of NIR and VIS OCT images from an acquired 3D data set, which consists of 512 × 128 A-scans. Also shown in the figure are the corresponding OCT fundus images, on which the locations of the OCT cross sectional images are marked. We can see that the contrast of the retinal blood vessels is higher in the VIS-OCT fundus

#152410 - $15.00 USD Received 4 Aug 2011; revised 12 Sep 2011; accepted 15 Sep 2011; published 22 Sep 2011

image due to the higher attenuation coefficient of the red blood cells in the VIS band. We can also see from the fundus images that the lateral resolution in the VIS band is better since we can recognize some small blood vessels that are not available in the NIR fundus image.

Owing to the depth resolving capability of OCT we can calculate the light reflection from a certain layer of the retina by summation of the OCT signals inside the layer:

$$I_{r(z_1 \sim z_2)}(x) = \sum_{z_1}^{z_2} I_{OCT}(x, z) \tag{1}$$

where I_{OCT} is the OCT intensity signal, x is the coordinates of the horizontal direction, z is the coordinates of the depth, z_1 and z_2 are the lower and upper boundaries of the layer. To calculate the reflections from the RNFL we first segmented the RNFL manually and calculated the reflection from inside the layer. We then calculated the ratio of the RNFL reflection over the fundus reflection calculated from the whole imageing depth using:

$$R_{RNFL} = \frac{I_{r(z_1 \sim z_2)}(x)}{I_{r(total)}}. \tag{2}$$

Figure 7 shows the segmentation of the RNFL boundaries in a pair of NIR and VIS OCT B-Scan images at the same location of the retina. Also shown in the figure are the calculated RNFL reflection ratios. From the calculation we can see that the reflection from the RNFL in the NIR band takes about 5% of the total fundus reflection. In the VIS band, however, the ratio increases to about 10%. The calculation shows that a higher portion of the fundus reflection comes from the RNFL reflection when imaged in the VIS band.

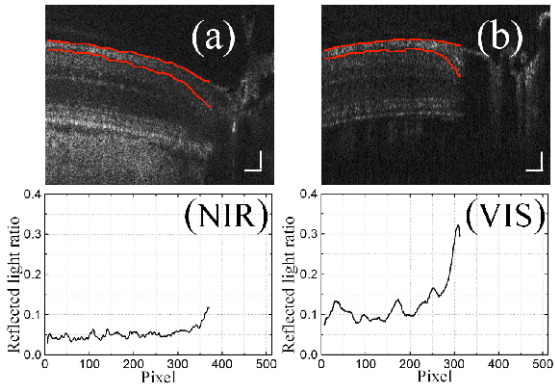

Fig. 7. Calculation of the ratio of RNFL reflection over the total fundus reflection for NIR (a) and VIS (b) OCT B-scans. Bar: 100 μm.

4. Conclusion

We have for the first time built a dual-band OCT system with one band centered at 415 nm and the other at 808 nm for imaging the spectral contrast of the RNFL. The system was successfully applied to imaging the rat retina *in vivo*. Significantly different appearances between the OCT cross sectional images at the two bands were revealed in the preliminary imaging tests. The experiments showed that a higher portion of the fundus reflection comes from the RNFL reflection when imaged in the VIS band. We can conclude that the dual-band OCT system is feasible for imaging the spectral contrast of the RNFL.

Acknowledgements

This work is supported in part by the following grants: National Institutes of Health grant 7R21EB008800-02 (Jiao), 1R01EY019951-01A1 (Jiao), and R01EY19084 (Huang) and Department of Defense grant W81XWH-11-1-0197 (Jiao).

#152410 - $15.00 USD Received 4 Aug 2011; revised 12 Sep 2011; accepted 15 Sep 2011; published 22 Sep 2011